Mathematical modelling and experimental simulation of chlorate and chlor-alkali cells.

Philip Byrne

ABSTRACT

The production of chlorate, chlorine and sodium hydroxide accounts for the largest part of electrochemical process production. As this relies on electrical energy, savings in this area are always a pertinent issue. Savings can be brought about through increased mass transfer of reacting species to the respective electrodes, and through increased catalytic activity and uniformity of current density distribution at these electrodes.

This thesis will present studies involving mathematical modelling and experimental simulations of these processes. They will show the effect that hydrodynamic behaviour has on the total current density and cell voltages, along with the effects on current density distributions and individual overpotentials at the respective electrodes.

Primary, secondary and psuedo-tertiary current density distribution models of a chlor-alkali anode are presented and discussed. It is shown that the secondary model presents current density distributions rather similar to the pseudo-tertiary model, although the potential distribution differs rather markedly. Furthermore, it is seen that an adequate description of the hydrodynamics around the anode is required if the potential distribution, and thereby the prevalence of side-reactions, is to be reasonable predicted.

A rigorous tertiary current density distribution model of a chlorate cell is also presented, which takes into account the developing hydrodynamic behaviour along the height of the cell. This shows that an increased flowrate gives more uniform current density distributions. This is due to the fact that the increased vertical flowrate of electrolyte replenishes ion content at the electrode surfaces, thus reducing concentration overpotentials. Furthermore, results from the model lead to the conclusion that it is the hypochlorite ion that partakes in the major oxygen producing side-reaction.

A real-scale cross-section of a segmented anode-cathode pair from a chlorate cell was designed and built in order to study the current density distribution in industrial conditions. These experiments showed that increased flowrate brought about more even current density distributions, reduced cell voltage and increased the total current density. An investigation of the hydrodynamic effects on the respective electrode overpotentials shows the anode reactions being more favoured by increased flowrate. This leads to the conclusion that the uniform current density distribution, caused by increased flowrate, occurs primarily through decreasing the concentration overpotential at the anode rather than by decreasing the bubble-induced ohmic drop at the cathode.

Finally, results from experiments investigating the bubble-induced free convection from a small electrochemical cell are presented. These experiments show that Laser Doppler Velocimetry is the most effective instrument for investigating the velocity profiles in bubble-containing electrochemical systems. The results also show that the flow can transform from laminar to turbulent behaviour on both the vertical and horizontal planes, in electrochemical systems where bubbles are evolved.

Keywords: Chlorate, chlor-alkali, current density distribution, current distribution, potential distribution, hydrodynamic behaviour, electrolysis, bubble-evolution.

THESIS CONTENT

I. Byrne P, Bosander P, Parhammar O, & Fontes E, "A primary, secondary and pseudo-tertiary mathematical model of a chlor-alkali membrane cell." *Jnl. Appl. Electrochem.,* **30** (2000) 1361.

II. Byrne P, Simonsson D, Lucor D, & Fontes E, "A model of the anode from the chlorate cell." Published in *Fluid Mechanics and its Applications* **Vol 51.** *Transfer Phenomena in Magnetohydrodynamic and Electroconducting Flows.* Alemany, Marty & Thibault editors. Kluwer, Dordrecht (1999).

III. Byrne P, Fontes E, Lindbergh G., & Parhammar O, "A simulation of the tertiary current density distribution from a chlorate cell. I: Mathematical model." *Accepted by J. Electrochem. Soc.* (2001).

IV. Byrne P, Fontes E, Cournet N, Herlitz F & Lindbergh G, "A simulation of the tertiary current density distribution from a chlorate cell. II: Experimental study." *Submitted to J. Electrochem. Soc.* (2001)

V. Boissonneau P, & Byrne P, "An experimental investigation of hydrogen gas bubble-induced free convection in a small electrochemical cell." *Jnl. Appl. Electrochem.,* **30** (2000) 767.

Also published by the author:

Bosander P, Byrne P, Fontes E, & Parhammar O, "Current distribution on a membrane cell anode." Published in *Chlor-Alkali and Chlorate Technology*, Burney, Furuya, Hine and Ota, Editors, **PV 99-21**, p. 45, The Electrochemical Society Proceedings Series, Pennington, NJ (1999).

Byrne P, Fontes E, Lindbergh G, & Parhammar O, "Experimental and computer simulations of the chlorate cell." Published in *Chlor-Alkali and Chlorate Technology*, Burney, Furuya, Hine and Ota, Editors, **PV 99-21**, p. 260, The Electrochemical Society Proceedings Series, Pennington, NJ (1999).

ACKNOWLEDGEMENTS

I would like to thank the following people, without which this thesis would not have been possible:

> Ed Fontes, your expertise has taught me a lot, your friendship has meant much and your drive has helped this thesis to be as structured and complete as it is. Also to Eva Nilsson, the softer side of Ed, thank you for your support and opinions.
>
> My supervisor, Göran Lindbergh, my office-mate, Anna-Karin Hjelm and the others from *Tillämpad Elektrokemi* for your opinions, support and for teaching me electrochemistry.
>
> Frederik Herlitz, H-G Sundström, Olof Parhammar, Mathias Strömberg and the others from EKA Chemicals, for the help in the experiments, electrochemistry and modelling.
>
> Ingemar Johansson, Martin Kroon and the guys from Permascand's *prototypverkstad*, for the design and construction of the experimental cells.
>
> Anders Dahlkild, Ruben Wedin, Fritz Bark and the others from *FaxénLaboratoriet*, for the advice and help with the hydrodynamics of the project. Furthermore, Patrick Boissonneau and Johan Persson, for showing me the experimental side of hydrodynamics.

The project was carried out at The Faxén Laboratory, a Competence Centre at The Royal Institute of Technology (KTH) supported by The Swedish National Board for Industrial and Technical Development (NUTEK), KTH and industrial partners. EKA Chemicals AB, Sundsvall, Permascand AB, Ljungaverk and Vattenfall Utveckling AB, Älvkarleby, are all acknowledged for the help given to this thesis.

Finally I would like to thank my fiancé, Åsa Sandström, and both our families for being there and for the support during the trying times. The thesis is dedicated to them and to the memory of Daniel Simonsson, who first taught me to appreciate electrochemistry.

LIST OF SYMBOLS

c	Concentration, mol m^{-3}
d_h	Hydraulic mean diameter, m
D	Diffusion coefficient, $m^2 s^{-1}$
F	Faraday's constant, A s mol^{-1}
g	Acceleration due to gravity, m s^{-2}
i	Current density, A m^{-2}
i_o	Exchange current density, A m^{-2}
i_{lim}	Limiting current density, A m^{-2}
k_l	Mass transfer coefficient, m s^{-1}
k	Rate of reaction
l	Cell depth, m
n	Unit normal vector perpendicular to the boundary
N	Mass flux, mol $m^{-2} s^{-1}$
r	Bubble radius, m
R	Production term, mol $m^{-3} s^{-1}$
R	Gas constant, J $mol^{-1} K^{-1}$
Re	Reynolds number
t	Time, s
T	Temperature, K
u	Ionic mobility, $m^2 V^{-1} s^{-1}$
u_{av}	Average velocity in cell gap, m s^{-1}
v	Velocity vector, m s^{-1}
w	Cell gap width, m
z	Valence
α	Transfer coefficient
η	Activation overpotential, V
ϕ, Φ	Potential field, V
κ	Conductivity, S m^{-1}
μ	Viscosity, N s m^{-2}
v	Gas evolution rate, $m^3 m^{-2} s^{-1}$
ρ	Density, kg m^{-3}
Ω	Domain label

Subscript / Superscripts

a, c	Anode / Cathode
b, ∞	Bulk solution domain
l, m	Liquid / metal
s	Domain close to electrode surface

CONTENTS

1. INTRODUCTION

Most industrial electrochemical processes are heavily reliant on mass transfer and how well reacting species move to and from electrode surfaces. This means that they are dependant on the mechanical energy inputs imposed through fluid flow and bubble evolution. Both these mechanisms are non-uniform throughout all electrolytic cells and, along with concentration variations, give rise to current density distributions.

These phenomena are present in the chlorate and chlor-alkali processes. Both entail extensive electrolyte flow throughout the cell geometry, and both include bubble production at the respective electrode surfaces. One of the major aims for these industries is to increase the uniformity of current density distribution in order to better utilize electrode surface area to reduce energy consumption and electrocatalyst depletion. A more uniform current density distribution also reduces the prevalence of side-reactions, e.g, oxygen gas and perchlorate.

This section will introduce the chlor-alkali and chlorate processes along with the effort that has previously been done in modelling the hydrodynamic behaviour and current density distribution of these systems. In addition, previously performed experimental work on current density distribution in electrolytic systems will be reviewed, along with experimental investigations of gas-evolving electrodes. Finally, the scope of this thesis will be presented.

1.1. The Chlor-alkali membrane cell and system

The chlor-alkali process produces chlorine and sodium hydroxide according to the following general equation:

$$2\mathrm{NaCl} + 2\mathrm{H_2O} \rightarrow 2\mathrm{NaOH} + \mathrm{H_2}(g) + \mathrm{Cl_2}(g) \qquad (1.1)$$

Hydrogen gas is produced at the cathode along with hydroxide ions, whilst chlorine gas is produced at the anode. The anolyte investigated in this thesis consists of 240 g l^{-1} NaCl and catholyte of 200 g l^{-1} NaOH at 353 K. An ion-exchange membrane divides the two compartments and allows ion transport to complete the electric circuit. Buoyancy of the respective bubbles drives an electrolyte replenishment process as the bubbles are steered through gaps between the electrode blades. These bubbles rise behind the blades and force fresh electrolyte to the electrode front through the same gaps, see Fig. 1.1.

Paper I investigated the 'lantern' cell structure found in ICI FM-21 electrolysers, previously presented in a paper by Martin and Wragg [1].

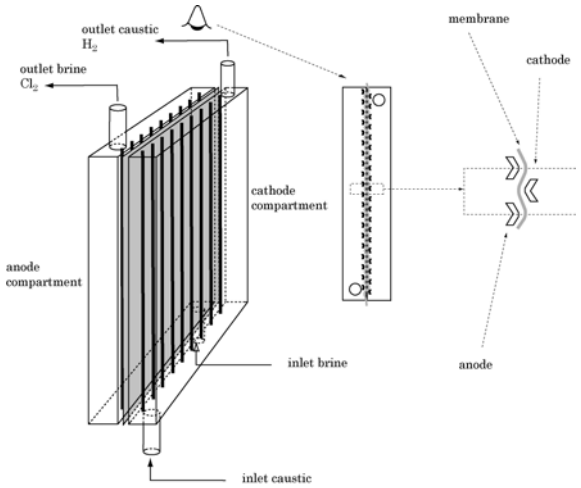

Fig. 1.1. A representation of a cell from the chlor-alkali process with the 'latern' cell structure.

The last few years has seen great improvements in cell design and materials and a remarkable increase in current density passing through chlor-alkali membrane cells [2]. This has led the process into areas where the electrolyte is significantly close to complete ion depletion, with all the subsequent problems of concentration overpotential and side-reactions that this incurs. By creating cell geometries or conditions that are favourable to a more uniform current density distribution, the production per unit electrode area is increased and the energy consumption per unit product is decreased. A uniform current density distribution also reduces localised corrosion and non-uniform depletion of electrocatalyst [3].

Primary current distribution models have previously been written to describe current density and potential distributions around the membrane cell anode [1, 4 & 5].

1.2. The Chlorate cell and system

The production of sodium chlorate ($NaClO_3$) occurs through the electrochemical oxidation of chloride ions and reduction of water from a brine solution (NaCl), according to the following basic equation:

$$NaCl + 3H_2O \longrightarrow NaClO_3 + 3H_2(g) \tag{1.2}$$

Sodium chlorate is the feedstock chemical to chlorine dioxide (ClO_2), a chemical used in 55% of the paper chemical bleaching processes [6]. A typical electrolyte contains 110 g l^{-1} NaCl, 600 g l^{-1} $NaClO_3$, 3 g l^{-1} NaOCl, and 3 g l^{-1} $Na_2Cr_2O_7$ at a maintained pH of 6.5, run at 343 K [7]. Chlorine is produced at the anode but never manages to form into bubbles, instead it reacts rather quickly to eventually produce the chlorate ion, see § 2.2. Oxygen gas bubbles, an unwanted by-product, are also produced at the anode and rob the system of 2% - 4% of the current [8]. A useful by-product, hydrogen gas, is formed at the cathode. The two electrodes are designed to be close to each other, with no inside separation.

Production occurs in large vessels, filled with brine and chlorate electrolyte, known as cell boxes, see Fig. 1.2. Cell boxes vary in size and shape but basically contain several electrode packets, each consisting of about 100 electrode pairs. An electrode pair is usually two 400 × 400 mm electrode surfaces, separated by a 3 mm cell gap. Usually, an assembly of chimneys is placed above the electrode packets to gather the hydrogen bubbles, with their buoyancy forcing electrolyte through the cell gaps. The lengths and geometries of these chimneys, along with the cell geometry, govern the velocity of electrolyte through the cell gaps.

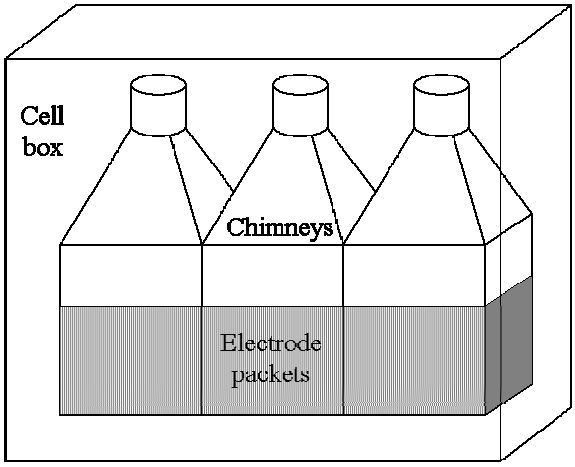

Fig. 1.2. A representation of a chlorate cell box with electrode packets and chimneys shown.

Ibl and Landolt [9 & 10] looked at chlorate and hypochlorite ion production through electrolysing concentrated and dilute chloride solutions, and presented one of the first mathematical investigations of this system. They assumed a constant diffusion layer thickness, calculated from the gas evolution rate at the anode [11 & 12]. Beck [13] looked at the macroscopic view of the process, and was able to extend the previous model to include a separated reactor, where the homogenous chemical chlorate formation could occur at different and more favourable conditions.

A flurry of investigations and model representations occurred during the seventies, where the chlorine molecule was still being industrially produced at graphite anodes. Jaksic and co-workers [14 – 19] furthered previous work and investigated the participating reactions in the concentrated states of industrial electrolytes. Their work did a lot towards defining the relevant physical properties in the unusual and extreme environment of an industrial chlorate electrolyte. Like Ibl and Landolt [11 & 12], they also assumed constant diffusion layer thicknesses and found averaged values in a small laboratory cell, using the limiting current density of the Fe^{2+}/Fe^{3+} redox couple.

Heal *et al.* [20] developed an iterative mathematical model to describe mass transfer and species concentrations. They combined the hydrodynamic diffusion layer, calculated through a relationship derived by Levich [21], and a bubble diffusion layer, found experimentally by Janssen and Hoogland [22], to describe mass transfer. Boxall and Kelsall [23] split the diffusion layer into two parts by an internal boundary. The first sub-domain involved the hydrolysis reaction existing in equilibrium, whilst the second assumed that this reaction was of the first-order and irreversible.

Vogt [24 & 25] empirically investigated the system and assumed that the cell acted like a plug-flow reactor. He concluded that the hypochlorite concentration decreased linearly from the inlet to the outlet, and that this could be used to define transport from the bulk to the respective electrodes. Ozil *et al.* [26] calculated the mass, voltage and mechanical energy balances of a chlorate cell by discretizing the channel length into a number of elementary-stirred electrochemical tank reactors. Wedin [27] modelled the global two-phase flow through a nominal cell box and electrode packet using a detailed two-phase model.

The model that is most similar to that presented in this thesis was developed recently by Leah *et al* [28]. They considered the pH profile between a flat anode and membrane in a system, from the chlor-alkali process, where flow had already developed into a laminar profile.

A moderate amount of experimental research into bubble-evolution and its effect on current density distribution has been performed over the years, although not a lot has been done using industrial-size laboratory cells. Funk and Thorpe [29] were one of the first to look at current density distribution using a segmented electrode, which they used to electrolyse water. Similar models and experimental work were done by a number of authors [30 – 34] and they all found that current density decreased along electrode height. Alkire and Lu [35] ran a series of experiments, where the electrode was not sectioned, by investigating mass transfer effects of a competing reaction at the gas-evolving electrode, the deposition of copper. All of the previous authors attributed the decrease of current density along electrode height to the electrical resistance brought about by bubble presence.

Gijsbers and Janssen [36] investigated the hydrodynamic behaviour and current density distribution properties of a water electrolysis cell by investigating the $Ag/Ag(CN)_2^-$ redox couple at the electrode. Their results showed a geometric decrease in current density along the leading part of the electrode, which became uniform along the higher parts of the electrode.

They concluded that gas evolution increased mass transfer locally, through the growing and detachment of bubbles, as well as globally, through the macro-convective properties of bubble-induced two-phase flow.

Czarnetzki and Janssen [37 & 38] were the first to investigate the current density distribution of a long cell in a chlorate/hypochlorite environment, with small cell gap. They found a trend of decreasing current density, from the leading edge along the electrode height, and concluded that current density distribution versus height was a linear relationship. Investigating the current density distribution itself, they found that this was more uniform at lower cell currents and greater flowrates. They also ran experiments where both the anode and cathode were segmented, and found that current density distribution was the same in both cases. Like the previous authors, they attributed the current density distribution behaviour to the increasing presence of bubbles along the electrode height.

1.3. Bubble-induced free convection in a small cell

Vogt [39] has given a summary of the work done on electrolytically-evolved gases. Electrolytically evolved bubbles are produced at electrodes in the dissolved state, where small nucleates start at imperfections in the electrode surface, and are then fed from the surrounding, highly supersaturated electrolyte [40 & 41]. Released bubbles continue to take in gaseous species from the surrounding electrolyte, growing in size as they rise through the channel. The fluctuant nature of turbulence, where bubbles travelling in direction collide with bubbles travelling in another, causes these bubbles to rupture and coalesce to form larger bubbles [42]. Coalescence has a significant effect on mass transfer and the electrochemical properties of a system [43].

The number of experimental investigations of electrolytically-evolved bubbles and their microconvective effects are rather limited, where the majority used cameras with rapid shutter speeds. Ziegler and Evans were the first to investigate a bubble-evolving, electrolytic system using laser-based velocimetry instruments [44].

1.4. The scope of the thesis

This thesis aims to present models and experimental simulations of current density distribution from the chlorate and chlor-alkali cells.

The thesis will firstly present two-dimensional primary, secondary and pseudo-tertiary current density distribution models around the lantern shape of a chlor-alkali anode and cathode pair (Paper I). Previous models have only considered the migratory properties of the chloride ion, whilst ignoring the convection and a complete description of the electrode kinetics. This investigation presents a model that also takes into account the kinetics of the chlorine reaction, as represented by an exponential relationship, and thus illustrate the distributions of current and potential in a secondary current density distribution model. The psuedo-tertiary model also considers the chloride ion transfer by firstly assuming a constant diffusion layer thickness around the anode shape. Finally, the gas-evolving diffusion layer model, developed by Ibl and Venczel [12], was used to define the diffusion layer thickness around the anode, and the investigation discusses the importance of this. The pseudo-tertiary current density distribution model is not a true tertiary model, as the mass transport characteristics of chlorine and migration of ions, in the diffusion layer, are not considered.

The thesis will then present a tertiary model of the chlorate cell. The majority of development in the chlorate industry has occurred through extensive experimentation on a myriad of possible system parameters and cell geometries. Yet, development is still required in areas such as the manufacturing of new electrocatalysts, in order to exclusively promote the desired reactions and lower the overpotential. Development is also required in the designing of new and novel cell geometries, in order to even out current density distribution and increase the mass transfer of species to and from the electrode surfaces. All of these improvements go towards achieving the overall desire of reducing energy consumption.

A true tertiary model was developed for the chlorate cell (Papers II and III), which solves and describes concentration profiles, mass transport and current density distributions, along the anode height, and illustrates these relationships using a developing velocity profile. The fact that convection is included in the model as a variable and developing phenomenon, is unique to studies of this type.

Many separate parameters are involved in the electrochemical production of sodium chlorate ($NaClO_3$). The thermodynamic and kinetic properties at the electrode surfaces, along with the physical properties of temperature, concentration and the hydrodynamic behaviour are intrinsically interrelated. The experimental simulation of a real-scale chlorate cell, presented in this thesis, will show how flowrate affects the current density distribution, anodic and cathodic overpotentials, cell voltage, total current density and diffusion layer thickness of this cell (Paper IV). It demonstrates that varying concentration overpotential has the greatest effect on current density distribution, more so than the presence of bubbles in the chlorate cell.

Finally, the thesis will investigate results from a gas-evolving electrolytic cell under conditions of natural convection (Paper V). The investigation measures the two-phase flow in a small cell composed of two flat-plate electrodes placed in a stagnant solution with a narrow cell gap. Bubble sizes, velocity profiles between the electrodes and gas fractions were determined through microscope-enhanced visualisation, Laser Doppler Velocimetry (LDV) and Particle Image Velocimetry (PIV). The results shed light upon the mechanisms of growing bubbles in industrial chlor-alkali or chlorate cells. They also show that it is possible to have transition from laminar to turbulent flow behaviour, both in a vertical and horizontal direction.

The investigations were chosen as initial studies of current density distribution of electrolytic systems that evolve bubbles. An understanding of the mechanisms that contribute to these distributions would lead to improvements of the systems and, essentially, a reduction in energy consumption. The first investigation (Paper I) develops the concept of current density distribution using simple models, although with a fairly complicated geometry from the chlor-alkali process. This investigation is expanded to develop a fully tertiary model (Papers II and III), with a less complex geometry.

The structure of the chlorate system enabled a vigorous and robust experimental investigation (Paper IV), in order to investigate and ratify the capabilities of its corresponding model. This paper was also useful in physically investigating the chlorate process at industrial scales and conditions. Finally, the investigation was expanded to observe the more complex issue of bubble-evolution, which is present in both processes (Paper V). The circumstances and abnormalities that this causes were investigated at a simple level, in order to pave the way for future modelling and experimental investigations that would include two-phase flow.

2. MATHEMATICAL MODELLING

This section will firstly present four models from the chlor-alkali system (Paper I) and then a tertiary model from the chlorate process (Papers II and III). In each case, the system chemistry is explained, the equations pertaining to the domain and boundaries are derived, and then the constants are found, manipulated and given.

2.1. The Chlor-alkali model

The chemistry

The geometry of a unit cell from the system is shown in Fig. 2.1, where a general depiction is given in Fig. 1.1. It is assumed that the mass transport properties and conductivity in the electrolyte and membrane remain constant throughout the system height, and from one slat to the next. It is also assumed that potential is constant throughout all metal structures.

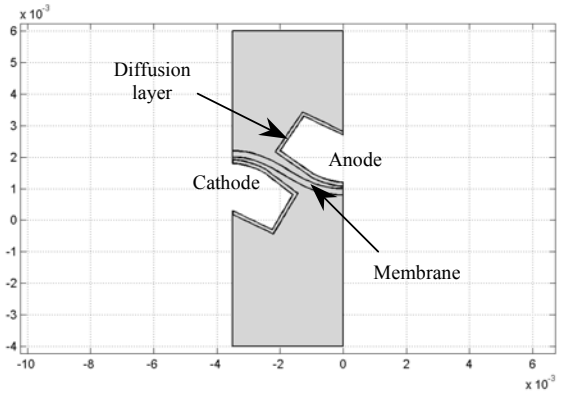

Fig 2.1. Unit cell geometry used in the respective models. A diffusion layer has been defined for use in the pseudo-tertiary current distribution model.

The chlor-alkali process evolves chlorine gas, at the anode, and hydrogen gas and hydroxide ions, at the cathode, according to the half-cell reactions:

$$2\mathrm{Cl}^- \rightarrow \mathrm{Cl}_2(g) + 2e^- \tag{2.1}$$

$$2\mathrm{H}_2\mathrm{O} + 2e^- \rightarrow 2\mathrm{OH}^- + \mathrm{H}_2(g) \tag{2.2}$$

The primary and secondary current density distribution models

The primary current density distribution model takes into account the migratory properties of ions in the electrolyte and membrane, and does not consider diffusion mass transport or the overpotential required to force the reactions to occur. The model is simplified by dividing the domain into three subdomains (denoted by Ω); the anolyte, membrane and catholyte. Ohm's law is assumed to adequately describe the ionic migration so that a current balance gives:

$$\nabla \cdot \left(-\kappa_j \nabla \phi\right) = 0 \qquad \text{in } \Omega_{all} \tag{2.3}$$

where ϕ denotes potential and κ_j conductivity. The subscripts j = 1, 2, 3, signify the anolyte, membrane and catholyte, respectively.

The boundary conditions assume potential to be constant at all of the electrodes, whilst net-mass fluxes through the boundaries at the top and bottom of the figure are assumed negligible, due to symmetry. Mass-flux at the boundaries, behind the electrodes, is also assumed to be negligible. This all results in the following equations:

$$\phi = \phi_a \qquad \text{at } \delta\Omega_a \tag{2.4}$$

$$\phi = \phi_c \qquad \text{at } \delta\Omega_c \tag{2.5}$$

$$-\kappa_j \nabla \phi \cdot \mathbf{n} = 0 \qquad \text{at } \delta\Omega_{other} \tag{2.6}$$

where **n** is the unit normal vector to the respective boundaries, ϕ is the potential, and the subscripts *a* denotes the anode and *c* the cathode.

The secondary current distribution model takes into consideration anode kinetics by introducing the activation overpotential, η:

$$\eta = \phi_m - \phi_l - \Delta\phi_{ml}^{eq} \tag{2.7}$$

where $\Delta\phi_{ml}^{eq}$ is the equilibrium potential of the anode reaction at the conditions of electrolysis, and the subscripts *l* denotes the electrolyte and *m* denotes the metal of the anode. Substituting this into equation (2.3) gives the relative anodic overpotential:

$$\nabla\eta = -\nabla\phi_l \tag{2.8}$$

The boundary condition at the anode is described by reaction kinetics that assume the desorption of chlorine is the rate determining step [45]:

$$\kappa_j \nabla\eta \cdot \mathbf{n} = i_o^b \left\{ \exp\left(\frac{\alpha_a F \eta}{RT} \right) - 1 \right\} \qquad \text{at } \delta\Omega_a \tag{2.9}$$

where i_0^b denotes the exchange current density, α_a the anodic transfer coefficient, *F* Faraday's constant, *R* the gas constant and *T* the temperature. The model assumes that the cathode reaction can be described reversibly, so that its boundary condition is:

$$\eta = \eta_{a-c} \qquad \text{at } \delta\Omega_c \tag{2.10}$$

where the term $\eta_{a\text{-}c}$ is the cathode potential relative to the anode. The other boundaries are still insulated:

$$\kappa_j \nabla\eta \cdot \mathbf{n} = 0 \qquad \text{at } \delta\Omega_{other} \tag{2.11}$$

Table 2.1 provides a summary of the data used in both the primary and secondary current distribution models. The electrolyte compositions and conditions are given in § 1.1, and the respective conductivities were calculated using this data. The models were run at the comparatively low current density of 3 kA m^{-2}. Membrane conductivity was obtained from Rondinini and Ferrari [46] and the kinetic data from Bard [45].

Table 2.1. Input data for the primary, secondary and pseudo-tertiary current density distribution models.

κ_1 / S m^{-1}	κ_2 / S m^{-1}	κ_3 / S m^{-1}	i_o / A m^{-2}	α_a	T / K
50	3	100	750	29	343

The pseudo-tertiary current distribution model

The pseudo-tertiary current distribution model takes into consideration chloride ion diffusion transport by assuming a constant, hypothetical diffusion layer around the anode. The presence of this diffusion layer adds a fourth subdomain to the system, which also includes the erroneous assumption that chloride ion transport only occurs through diffusion, as if it existed in a supporting electrolyte [5].

Mass transport due to diffusion is only taken into account in the fourth subdomain, so that the equations describing the other three subdomains remain unchanged. Once again, the production of charge does not occur:

$$\nabla \cdot \left(\kappa_j \nabla \phi \right) = 0 \qquad \text{in } \Omega_{all} \qquad (2.12)$$

As there is a further boundary between the anolyte and diffusion layer subdomains, constant concentrations are set in the first three subdomains:

$$c = c_j^{\circ} \qquad \text{in } \Omega_j \qquad (2.13)$$

for the subdomains; j = 1, 2, 3, where c° is set to 4 100 mol m^{-3} (j = 1), in the anolyte, and set to zero in the other two subdomains. Concentration is the variable factor in the diffusion layer subdomain (j = 4), so that the conservation of mass yields:

$$\nabla \cdot \left(- D_1 \nabla c \right) = 0 \qquad \text{in } \Omega_4 \qquad (2.14)$$

where D_1 represents the diffusion coefficient of chloride in the diffusion layer.

The kinetic expression (Eqn. 2.9) at the anode has to take into account chloride ion concentration at the surface, and is rewritten as:

$$\kappa_j \nabla \eta \cdot \mathbf{n} = i_{\mathrm{o}}^{b} \left\{ \left(\frac{c}{c^b} \right)^2 \exp\left(\frac{\alpha_a F \eta}{RT} \right) - 1 \right\} \qquad \text{at } \delta\Omega_a \qquad (2.15)$$

where c^s is the concentration of ions at the surface and c^b is the concentration at the reference state. Using Faraday's law, Eqn. (2.15) can be expressed as a mass balance, and the anode boundary conditions are:

$$-D_{\mathrm{l}} \nabla c \cdot \mathbf{n} = -\frac{1}{F} i_{\mathrm{o}}^{b} \left\{ \left(\frac{c}{c^b} \right)^2 \exp\left(\frac{\alpha_a F \eta}{RT} \right) - 1 \right\} \quad \text{at } \delta\Omega_a \qquad (2.16)$$

The other boundary conditions are those of the secondary current density distribution model, expressed by Eqns. (2.10) and (2.11). The pseudo-tertiary current density distribution model uses input data given in Table 2.1, and the subsequent data in Table 2.2.

Table 2.2. Additional input data for the pseudo-tertiary current density distribution model.

$c_{\mathrm{l}}^{\mathrm{o}}$ / mol m^{-3}	$c_{\mathrm{l}}^{\mathrm{o}}$ / mol m^{-3}	$c_{\mathrm{l}}^{\mathrm{o}}$ / mol m^{-3}	D_{l} / m^2 s^{-1}
4100	Not conditioned	0	1e-9

The extended secondary current density distribution model

A simplified analytical model, or extension to the secondary model, that also considers the transport of chloride ions was investigated. The limiting current density is a way of expressing the influence that the diffusion layer thickness has on ion transport to the electrode surface. The equations for the boundary conditions are those used in the secondary current distribution model, except for Eqn. (2.9). This was found by using the following analytical expression, which is applicable for ion transport in a supporting electrolyte [47]:

$$\kappa_1 \nabla \eta \cdot \mathbf{n} = \frac{i_o^b \left\{ \left(\frac{c}{c^b} \right)^2 \exp\left(\frac{\alpha_a F \eta}{RT} \right) - 1 \right\}}{1 + \frac{\exp\left(\frac{\alpha_a F \eta}{RT} \right)}{i_{\lim}^{ox}}} \qquad \text{at } \delta\Omega_a \qquad (2.17)$$

where $i_{\lim}^{ox}$ is the limiting current density for the oxidation of chloride ions. The expression differs from Eqn. (2.15) in that it gives the current density distribution as a function of potential and limiting current density.

The approximation of diffusion layer due to gas evolution

The work of Ibl and Venczel [11 & 12] has led to a simple equation that describes how mass transport to an electrode surface is affected by bubble evolution. They found the mass transfer coefficient, k_1, to be a property of bubble evolution rate, bubble size and the ionic transport:

$$k_1 = 2\sqrt{\frac{D_1}{\pi\tau}} \qquad (2.18)$$

where D_1 is the chloride ion diffusion coefficient, and:

$$\tau = \frac{2r}{3v} \qquad (2.19)$$

where r is the bubble radius and v is the gas evolution rate per unit area.

2.2. The Chlorate model

The chemistry

The reaction scheme for the production of sodium chlorate involves the following electrochemical and ordinary chemical reactions [48]:

$$2Cl^- \Leftrightarrow Cl_2(aq) + 2e^- \tag{2.20}$$

$$Cl_2(aq) + H_2O \underset{k_3^b}{\overset{k_3^f}{\Leftrightarrow}} HOCl + Cl^- + H^+ \tag{2.21}$$

$$HOCl \underset{k_4^b}{\overset{k_4^f}{\Leftrightarrow}} OCl^- + H^+ \tag{2.22}$$

$$2HOCl + OCl^- \underset{k_5^b}{\overset{k_5^f}{\Leftrightarrow}} ClO_3^- + 2H^+ + 2Cl^- \tag{2.23}$$

where k represents the rate of reaction in either the forward (f) or backward (b) directions. Chloride ions are oxidised at the anode surface to chlorine, which in turn hydrolyses quite rapidly to hypochlorous acid. This reacts to the hypochlorite ion, and both ions can be transported to the bulk or back to the anode surface. There also exists a number of side-reactions that occur both electrochemically and chemically, and are explained in more detail by Boxall and Kelsall [23]. The main side-reaction is given by the electrochemical decay of the hypochlorite ion [49]

$$ClO^- + H_2O \Leftrightarrow Cl^- + 2H^+ + O_2(g) + 2e^- \tag{2.24}$$

Alternatively, if we added a proton to both sides of this reaction, the side-reaction could be described by the electrochemical decay of the hypochlorous acid molecule [50]:

$$HClO + H_2O \Leftrightarrow Cl^- + 3H^+ + O_2(g) + 2e^- \tag{2.25}$$

Further side-reactions are the decay of the hypochlorite ion [49]:

$$2OCl^- \underset{k_8^b}{\overset{k_8^f}{\Leftrightarrow}} 2Cl^- + O_2(g) \tag{2.26}$$

and the electrochemical splitting of water:

$$2H_2O \Leftrightarrow O_2(g) + 4H^+ + 4e^- \tag{2.27}$$

The chemical decay of hypochlorite ions, Eqn. (2.26), is catalysed by the anode, metal ions or impurities in the electrolyte, without the transfer of electrons. It is considered here as being a homogenous reaction that can occur anywhere throughout the model domain. As both hydrogen and hydroxide ions are considered in the model, the following reaction is also accounted for:

$$H^+ + OH^- \underset{k_7^b}{\overset{k_7^f}{\Leftrightarrow}} H_2O \tag{2.28}$$

Finally, the model takes into account the electrochemical production of hydrogen at the cathode,

$$2H_2O + 2e^- \Leftrightarrow H_2(g) + 2OH^- \tag{2.29}$$

where it is assumed that this reaction occurs at a 100% current efficiency. This would be the case if sodium dichromate were included, as it forms a protective layer at the cathode, although this ion is not considered in the mathematical model. A schematic representation of the participating reactions and side-reactions, and where they occur in the reaction domain is given in Fig. 2.2.

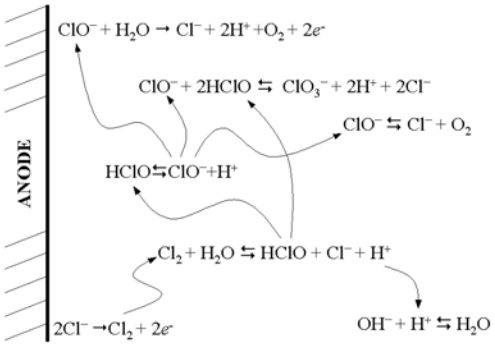

Fig. 2.2. Schematic representation of the participating reactions and species in the chlorate process.

The Model

The models considers the three fundamental transport mechanisms; diffusion, migration and convection, for all nine species in the Nernst-Planck equation [5]:

$$\mathbf{N}_i = -D_i \nabla c_i - z_i F u_i c_i \nabla \Phi + \mathbf{v} c_i \tag{2.30}$$

where D_i is the diffusion coefficient, u_i is ionic mobility and z_i is electrical charge of species i, F is Faraday's constant, Φ is the potential field and $\mathbf{v}$ is the velocity vector. It solves the following mass balance for each of the species at steady state:

$$-\nabla \cdot \mathbf{N}_i + \mathrm{R}_i = 0 \tag{2.31}$$

where c_i is concentration, $\mathbf{N}_i$ is mass transfer flux and R_i is the production term of species i, whilst t is time. In order to get the same amount of dependant variables as equations, the electroneutrality condition is used:

$$\sum_i z_i c_i = 0 \tag{2.32}$$

Electrolyte flow is assumed to enter the cell gap with a uniformly distributed velocity profile over the cell gap. The model finds the velocity vector, $\mathbf{v}$, through solving the Navier-Stokes equations [51], at steady state:

$$\rho\left(v_x \frac{\partial \mathbf{v}}{\partial x} + v_y \frac{\partial \mathbf{v}}{\partial y}\right) = -\nabla p + \mu \nabla^2 \mathbf{v} + \rho g \tag{2.33}$$

with the continuity equation:

$$\nabla \cdot \mathbf{v} = 0 \tag{2.34}$$

The hydrodynamic behaviour is assumed to be constant throughout the depth of the cell, z – direction, whilst the effect of bubble evolution on electrolyte volume and ohmic resistance is neglected.

The boundary equations

The reactions at the boundaries are calculable from the Nernst-Planck expression for flux, and Faraday's law:

$$\mathbf{N}_i \cdot \mathbf{n} = \frac{1}{nF} i_i \tag{2.35}$$

where i is the current density of the charge transfer reactions, Eqns. (2.20), (2.24), and (2.27), at the electrode. These are described by the following Butler-Volmer equations, respectively:

$$i_2 = i_{0,2}\left[\left(\frac{c^s_{\mathrm{Cl^-}}}{c^\infty_{\mathrm{Cl^-}}}\right)^2 \exp\left\{\frac{2F}{RT}\left[\left(\Phi_m - \Phi_l\right) - \Delta\Phi^\mathrm{o}\right]\right\} - \left(\frac{c^s_{\mathrm{Cl_2}}}{c^\infty_{\mathrm{Cl_2}}}\right)\right] \tag{2.36}$$

$$i_9 = i_{0,9}\left(\frac{c^s_{\mathrm{OCl^-}}}{c^\infty_{\mathrm{OCl^-}}}\right)\exp\left\{\frac{0.5F}{RT}\left[\left(\Phi_m - \Phi_l\right) - \Delta\Phi^\mathrm{o}\right]\right\} \tag{2.37}$$

$$i_{13} = i_{0,13}\left(\frac{c^s_{\mathrm{H^+}}}{c^\infty_{\mathrm{H^+}}}\right)^{-1} \exp\left\{\frac{1.5F}{RT}\left[\left(\Phi_m - \Phi_l\right) - \Delta\Phi^\mathrm{o}\right]\right\} \tag{2.38}$$

where i is current density, $i_{0,2}$ is the exchange current density, c is concentration, F is Faraday's constant, R is the universal gas constant, T is absolute temperature, Φ is the actual potential and $\Delta\Phi^\mathrm{o}$ is the standard equilibrium potential. The superscripts, ∞ and s, relate to the electrolyte in the bulk and at the anode surface, respectively.

Eqn (2.36) is valid on the assumption that the recombination of adsorbed chlorine species discharge is rate determining [52], whilst Eqn (2.37) is assumed to be a first-order reaction and Eqn (2.38) assumes that the hydrogen ion discharge step is rate determining [53]. Eqn (2.37) is used throughout except when the hypochlorous acid molecule is investigated as a participant in a side-reaction, where the equation is then exchanged with the first-order equation:

$$i_{11} = i_{0,11}\left(\frac{c^s_{\mathrm{HOCl}}}{c^\infty_{\mathrm{HOCl}}}\right)\exp\left\{\frac{0.5F}{RT}\left[\left(\Phi_m - \Phi_l\right) - \Delta\Phi^\mathrm{o}\right]\right\} \tag{2.39}$$

Certain species in the electrolyte do not undergo any charge transfer reaction so that at the boundaries:

$$\mathbf{N}_i \cdot \mathbf{n} = 0 \tag{2.40}$$

where **n** is the vector perpendicular to the boundary.

The constants and input data

The diffusion and migration terms from the Nernst-Planck equation contain the diffusion and ionic mobility constants, which are assumed as being uniform throughout the model domain. The diffusion coefficients for Cl^-, OH^-, Na^+ and ClO_4^- are all taken from Newman [5], where it is assumed that ClO_3^- can be expressed by the properties of the perchlorate ion, ClO_4^-. The diffusion coefficients for HOCl, OCl^- and $Cl_2(aq)$ are all taken from Chao [54]. The respective diffusion coefficients and ionic mobilities are all computed to the conditions of an industrial electrolyte, as explained in Paper III, and given in Table 2.3. The ionic mobilities can be calculated from the Nernst-Einstein-type equation given in this paper.

Table 2.3. Diffusion coefficients and inlet concentrations of the electrolyte species.

Species	Diffusion Coefficient	Concentration
Chloride ion	1.71×10^{-9} m^2 s^{-1}	1.88×10^{3} mol m^{-3}
Aqueated Chlorine	1.83×10^{-9} m^2 s^{-1}	8.66 mol m^{-3}
Hypochlorous acid	1.11×10^{-9} m^2 s^{-1}	4.30×10^{1} mol m^{-3}
Hypochlorite ion	1.07×10^{-9} m^2 s^{-1}	2.42×10^{1} mol m^{-3}
Hydrogen ion	7.86×10^{-9} m^2 s^{-1}	3.16×10^{-7} mol m^{-3}
Hydroxide ion	4.43×10^{-9} m^2 s^{-1}	4.79×10^{-7} mol m^{-3}
Chlorate ion	1.51×10^{-9} m^2 s^{-1}	5.63×10^{3} mol m^{-3}
Aqueated Oxygen	Not applicable	5.80×10^{-3} mol m^{-3}
Sodium ion	1.11×10^{-9} m^2 s^{-1}	7.54×10^{3} mol m^{-3}

The production term, R_i, of Eqn. (2.30) is common to the homogenous chemical reactions given in Eqns. (2.21), (2.22), (2.23), (2.26) and (2.28), and can be expressed in the following stoichiometric equation:

$$aA + bB \underset{k_j^b}{\overset{k_j^f}{\Longleftrightarrow}} cC + dD \tag{2.41}$$

If the interesting component from this equation was C, then the production term is expressed as:

$$R_C = k_C^f c_A^a c_B^b - k_C^b c_C^c c_D^d \tag{2.42}$$

Despic *et al.* [16] found the forward rate of the hydrolysis reaction (2.21). A rate for the hypochlorous acid molecule association reaction, Eqn. (2.22), was not found in the literature, so that the rate of re-association is assumed to be that of water, Eqn. (2.28). Water's re-association constant is taken from Moore [55]. Peters [56] found the forward rate of reaction and equilibrium constant from the chlorate forming reaction, Eqn. (2.23). Once again, no data for the rates of reaction of hypochlorite decay, Eqn. (2.26), were found, so that the rate of manganese-catalysed hypochlorite decay found by Lister [57] is taken. The forward and backward rates of all the reactions are re-calculated to the conditions of an industrial electrolyte, as described in Paper III, and listed in Table 2.4.

Table 2.4. Kinetic data for the homogenous chemical reactions.

Equation	Forward Rate (k^f)	Backward Rate (k^b)
2.21	$2.08\ s^{-1}$	$6.74\times10^{-2}\ m^6\ mol^{-2}\ s^{-1}$
2.22	$7.70\times10^{-1}\ s^{-1}$	$1.40\times10^{3}\ m^3\ mol^{-1}\ s^{-1}$
2.23	$1.80\times10^{-8}\ m^6\ mol^{-2}\ s^{-1}$	$5.00\times10^{-8}\ m^{12}\ mol^{-4}\ s^{-1}$
2.26	$1.06\times10^{-6}\ m^3\ mol^{-1}\ s^{-1}$	$1.40\times10^{-13}\ m^3 mol^{-1} s^{-1}$
2.28	$2.12\times10^{-7}\ s^{-1}$	$1.40\times10^{1}\ m^3\ mol^{-1}\ s^{-1}$

The final input terms in the mass balance equations (2.30) are the respective inlet concentrations. The industrial electrolyte composition listed in § 1.2 is used, and the input parameters can be either directly calculated, or found from the forward and backward rates of reaction listed above, see Paper III.

Input parameters in the electrochemical boundary equations are very dependant on the conditions of an electrolyte and the state and electrode material compositions. The respective exchange current densities and equilibrium electrode potentials, used in the model are listed in table 2.5. The values for chlorine production and water splitting were chosen arbitrarily, but to be of the same order of magnitude as those reported by Bard [45]. The electrochemical decay of the hypochlorite ion, Eqn. (2.24), is difficult to investigate, and the actual kinetics in an industrial electrolyte have never been found or postulated, to the knowledge of the authors. The equilibrium electrode potential was taken from Kotowski and Busse [50], while the exchange current density was adjusted so as to guarantee a 2% - 4% production of oxygen. The same equilibrium potential was used when the hypochlorous acid molecule was assumed to electrochemically decay, Eqn. (2.25), and the exchange current density was also adjusted to guarantee the same oxygen production.

Table 2.5. Equilibrium electrode potentials and exchange current densities for the heteregenous electrochemical reactions.

Equation	Equilibrium Potential	Exchange Current Density
2.36	1.36 V	1.0 A m^{-2}
2.37	0.96 V	2.5×10^{-9} A m^{-2}
2.38	1.23 V	2.0×10^{-6} A m^{-2}
2.39	0.96 V	4.5×10^{-12} A m^{-2}

The boundary conditions for the hydrodynamic equations (Eqns. (2.33) and (2.34)) are a given uniform inlet velocity, no slip condition at the two electrodes, and a constant pressure at the outlet.

The model is two-dimensional and assumes no variations in the direction of cell depth. The height was set to 400 mm and cell gap width to 3 mm. The model numerically solves the system by applying a finite difference method, using sparse matrix routines included in MATLAB®.

3. EXPERIMENTAL

Experimental investigations were done in order to examine the respective systems and test the validity of the models. This section will summarise the methods of experimental investigations presented in two papers. The first investigated the effect of flowrate on the current density distribution and other electrochemical behaviour of a real-scale cross-section of a chlorate cell (Paper IV). These investigations were run by imposing either a constant total current (hitherto known as galvanostatic trials), or a constant cell voltage (hitherto known as potentiostatic trials). The other paper investigated a small electrolytic cell in stagnant sodium sulphate and sodium chlorate electrolytes (Paper V). Optical and laser techniques were used to study the bubbles and hydrodynamic behaviour of this cell.

3.1. The Chlorate cell experiments

Four different sets of trials were run using the chlorate cell:

1. Cathodic and anodic voltage investigations: In order to examine the hydrodynamic effects on the relationship between the cathodic and anodic voltages, potentiostatic and galvanostatic trials were run where voltage between the respective electrodes, and a reference electrode placed at a point halfway within the cell gap was measured.
2. Cell current and voltage investigations: In order to investigate the hydrodynamic effects on the total current, cell voltage and current density distributions of the cell, potentiostatic and galvanostatic trials were run. The physical conditions of an industrial chlorate electrolyte were reached before voltage was applied, and the LABVIEW program controlled the cell voltage.
3. Pressure drop investigations: In order to study the global hydrodynamic behaviour of the cell, pressure drop was measured between the two pressure measurement points along the cell height. Flowrate was changed for the cases of an electrolysed and non-electrolysed chlorate electrolyte.
4. Iron (II/III) hexacyanide investigations: In order to test the hydrodynamic behaviour of the cell in a simplified and controlled environment, an electrolyte containing $K_3Fe(CN)_6$ and $K_4Fe(CN)_6$ was electrolysed. Voltage was applied and controlled directly from the rectifier, whilst cell voltage and current was measured in order to find the limiting current.

The cell and system were built in order to achieve the same temperatures, electrolyte compositions, current densities, pressure drops and flow of a real cell. The investigated electrolytes contained 560 – 600 g l^{-1} of $NaClO_3$, 100 – 110 g l^{-1} NaCl and 2 – 5 g l^{-1} NaOCl. 30 – 40 l of these electrolytes were mixed and maintained at a constant temperature of 60° - 70° C in a holding tank. The pH could be lowered to a range of 6.5 - 7.5 through metered addition of HCl, prior to the cell. A further series of trials were run where the $Fe(CN)_6^{3-}$ and $Fe(CN)_6^{4-}$ ions were electrolysed. An electrolyte containing 1 M KOH , 0.1 M $K_3Fe(CN)_6$ and 0.1 M $K_4Fe(CN)_6$ was pumped through the system at 24° – 25° C, see Fig. 3.1.

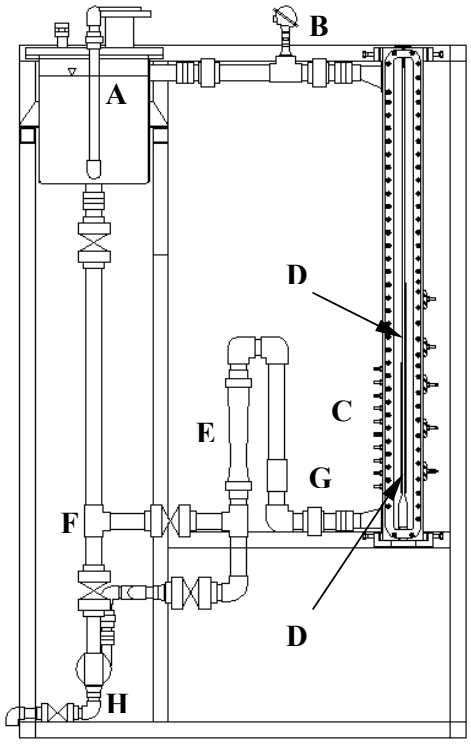

Fig. 3.1. Detailed drawing of the chlorate cell and surrounding assembly. A. Holding tank. B. Temperature reading point. C. Sectioned electrodes. D. Pressure reading points. E. Flowmeters. F. Acid entry point. G. pH reading point. H. Pump.

The total cell was approximately 2 m in height and electrolyte entered a chamber deemed large enough to settle it before entering the gap. The cell had electrode heights of 400 mm, that were 40 mm in depth, and a cell gap of 3 mm was set between the electrodes. Electrolyte samples could be taken from points just before the inlet chamber, and just after the outlet chamber.

The method for measuring current density distribution, cell voltage, anodic and cathodic voltages and pressure drop are explained in Paper IV. Polarizing the electrolyte of $Fe(CN)_6^{3-}$ and $Fe(CN)_6^{4-}$ ions gave a limiting current density, which could then be used to calculate the diffusion layer thickness, as also explained in Paper IV.

3.2. The Small electrochemical cell experiments

Three different sets of trials were run using the cell:

1. Microscope enhanced visualisation: to determine bubble sizes and concentrations.
2. Laser Doppler Velocimetry (LDV): to measure velocity profiles and turbulent intensity in the cell gap.
3. Particle Image Velocimetry (PIV): to visualise the global behaviour of the two phase flow.

The experiments were run on a small, Plexiglas vertical cell, 120 mm long and 30 mm wide, in which the two plate electrodes, 40 mm x 30 mm, were embedded, as shown in Fig. 3.2. Two thin glass plates were placed on the sides of the Plexiglas walls in order to enclose the cell gap and force the electrolyte to enter from beneath. The cell sat in 5 l of 50 g l^{-1} Na_2SO_4 electrolyte, for the investigation of water splitting, and 5 l of 50 g l^{-1} NaCl / 200 g l^{-1} $NaClO_3$ electrolyte when investigating chlorate production. Hydrogen was produced on a coated titanium cathode in both systems, whilst two types of DSA® electrodes, coated respectively with chlorine and oxygen evolving electrocatalyts, were used as anodes. All the different measurement techniques investigated the current densities: j = 500, 1000, and 2000 A m^{-2}.

Microscope enhanced visualisation involved a stroboscopic light being focused by a convergent lens into the region of the measurement volume, through a method similar to Boissonneau [58]. A bubble counting method was used, where images were digitised and controlled by the NIH Scion Image 1.62 software package. Further equipment details are given in Paper V.

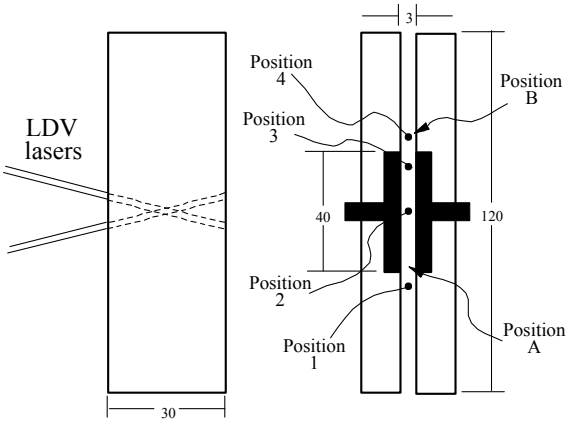

Fig. 3.2. Cell dimensions, LDV arrangement and positions for the visualisation trials (Positions A and B) and for the LDV trials (Positions 1 - 4).

Bubble and fluid velocities were measured in the cell gap using LDV, at different heights along the cell length, as shown in Fig. 3.2 and explained in Paper V. LDV was used to measure the extent of turbulent behaviour in the small electrochemical cell. It does this by measuring velocity fluctuations, which is a measure of the extent of deviations occurring from the mean velocity of a flow, see Paper V. PIV was also used to find the point where laminar behaviour transferred to turbulent behaviour. The camera was placed perpendicular to a laser sheet, shone from below, which crossed the cell gap perpendicular to the electrodes. Its details are also discussed in Paper V.

4. RESULTS AND DISCUSSION

The following section is a summary of the results and discussion from all of the papers presented in this thesis. It will start out by presenting results from the chlor-alkali model (Paper I). It will then present the results from the chlorate model (Papers II and III) along with those from the experimental simulation of a chlorate cell (Paper IV). In this respect, a comparison of the results from experiment and the model will bring about a discussion of their validity. Finally, this section will present results from experiments run on a small electrochemical cell (Paper V).

4.1. The Chlor-alkali model

Results from the primary and secondary current distribution models

A primary and secondary model are firstly presented in order to show the effects of ion conductivity, and electrode kinetics. These can be compared to the effects of mass transfer from the pseudo-tertiary model. Fig. 4.1 shows results from the primary and secondary current distribution models where potential is represented by the height of the diagram, and current density by the flowlines. The diagrams show that the major potential drop occurs through the membrane, and that this poor membrane conductivity works in equalising the distribution. The figure also shows that membrane and electrolyte conductivities have a far greater influence on the current density distribution than the electrode kinetics does. This is understandable as the chlorine reaction is very fast and has a high exchange current density.

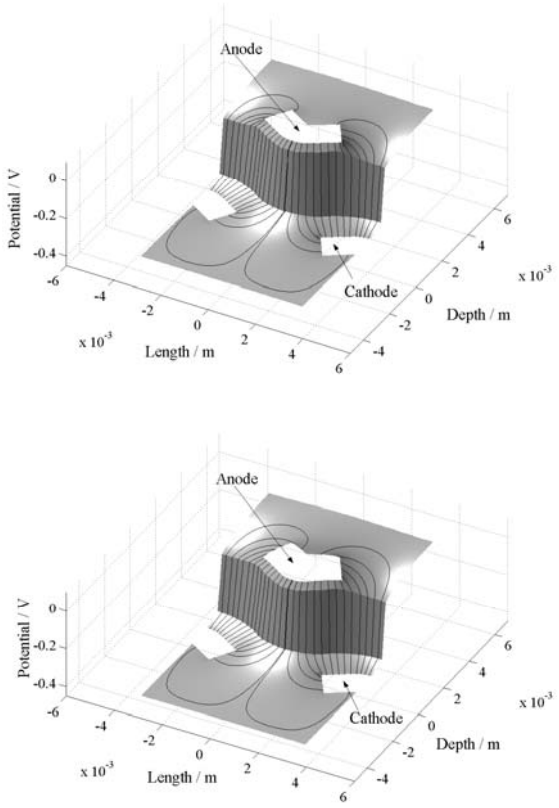

Fig. 4.1. Three dimensional view of the primary (top) and secondary current density (bottom) and potential distributions at the anode and cathode surfaces.

A view of the overpotential in the secondary current density distribution model is seen in the left diagram of Fig. 4.2. Current density distribution in the secondary model is seen in the left diagram of Fig. 4.3. The introduction of the reaction kinetics has hindered the electrode reactions to the extent that reactions have started occurring at the anode back.

Results from the pseudo-tertiary current distribution model

The right diagrams in Figs. 4.2 and 4.3 show the potential and current density distributions from the pseudo-tertiary current distribution model, respectively. The pseudo-tertiary model takes into account the mass transport of chloride ions, which means that concentration overpotential is required to transport the species to the anode surface. Fig. 4.2 clearly shows that overpotential is far greater in the pseudo-tertiary model than the secondary model and that this increase is more pronounced at the back. This has the effect of sending more current density to the anode back, noticeable in Fig. 4.3.

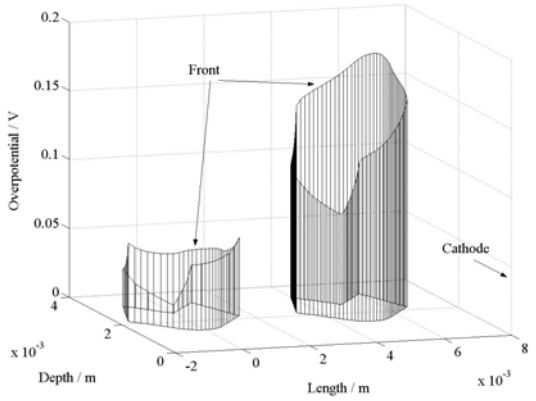

Fig. 4.2. Potential distribution in the solution at the anode surface for the secondary (left) and pseudo-tertiary current distribution model (right) cases.

The fact that overpotential on the anode back is far lower than at the front is due to the assumption that diffusion layer thickness is constant. This results in a failure to consider the real convective properties of the system and the effect that gas evolution would have on ionic transport close to the anode. Taking these into account would mean that there would be an average diffusion layer that is thinner at the front, where gas-evolution is more prevalent, than at the back.

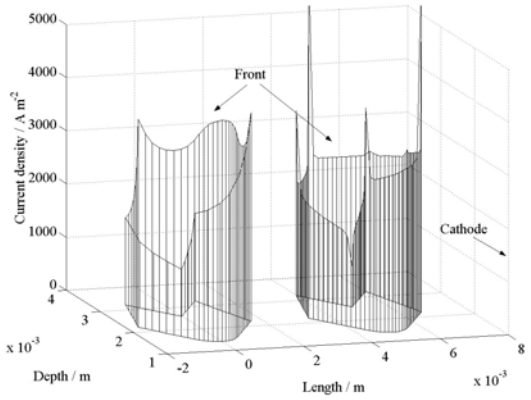

Fig. 4.3. Current density distribution at the anode (perpendicular to the surface) for the secondary (left) and pseudo-tertiary (right) current density distribution model cases.

Using the model of Ibl and Venczel [11 & 12] (Eqns. 2.18 and 2.19), the diffusion layer thicknesses at a variety of current densities could be calculated. The effect of varying diffusion layer thicknesses on current density distribution was limited (Paper I), but significant on the overpotential distribution, as seen in Fig. 4.4. This shows that overpotential decreases considerably at the anode front when the diffusion layer thickness is halved. If we were to postulate that gas evolution imposes a diffusion layer thickness of 8.2 μm at the anode front, whilst the thickness is still 100 μm at the back, then the model would show the overpotential being basically uniform around the whole of the anode (Paper I). This shows that the variability of diffusion layer thickness should be considered in order to achieve a reasonable description of the potential distribution, and the positions of side-reactions that can therefore occur.

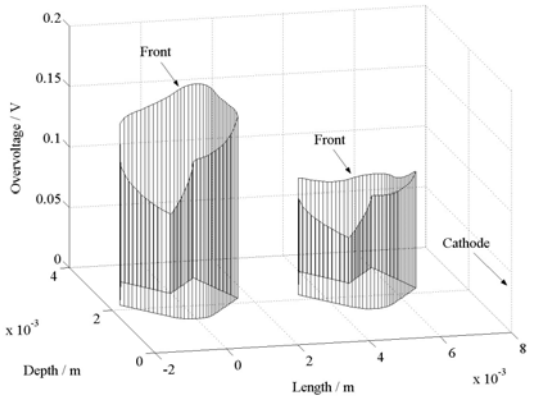

Fig. 4.4. Potential distribution at the anode for the pseudo-tertiary current distribution model, where the diffusion layer thickness is set to 100 μm (left) and 50 μm (right).

Comparison between the pseudo-tertiary current distribution and the analytical mass transport limitation models

A simpler way of computing the effect of mass transfer is to extend the secondary model using the concept of i_{lim} to represent the mass transfer affects in the model, Eqn. (2.17). It is a lot easier to express i_{lim} as a function of either position, current or gas evolution rate than it is to change the geometry system every time a different case is to be investigated, which must be done in the pseudo-tertiary model. Fig. 4.5 shows that current density distributions are similar from both models as is the case when comparing the potential distributions (Paper I). The analytical model is quite decent as an initial indication of current density distribution, but relies heavily on the assumption of the presence of a supporting electrolyte. Only the pseudo-tertiary current distribution model has the potential to be developed in order to include this, and all of the other assumptions used in the described models.

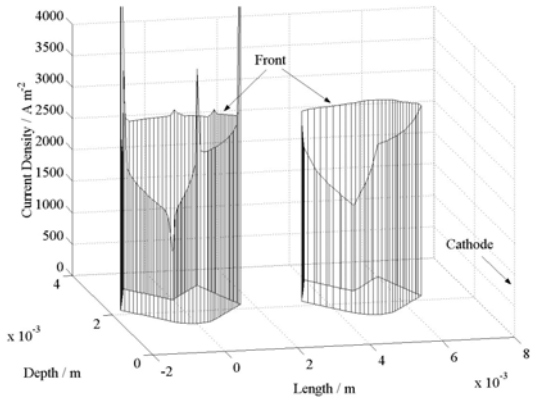

Fig. 4.5. Current density distribution at the anode (perpendicular to the surface) for the pseudo-tertiary current distribution model (left) and the analytical mass transport limitation model (right), where the diffusion layer thickness is set to 100 μm and the concentration bulk is 4100 mol m^{-3}.

4.2. The Chlorate model

This model simulates a number of the chlorate system properties, especially the current density distribution, as functions of electrolyte velocity and exchange current density. It also investigates the issue of which species are actually taking part in the side-reactions at the anode.

Concentration profile and current density distribution

Fig. 4.6 shows a contour plot of the electrolyte velocity development from its uniform flat-line profile at the cell gap entrance. Viscous friction from the electrode surfaces leads to a viscous layer developing along the height of each of the electrodes, resulting in an evolving parabolic laminar velocity profile across the cell gap. An appropriate description of the system hydrodynamics is imperative, as there occurs a significant development of flow throughout the cell height.

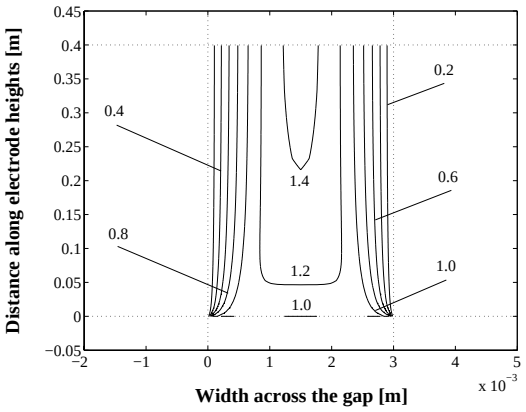

Fig. 4.6. Development of the velocity profile with an inlet straight-line velocity of 1.0 ms^{-1} at the cell gap entrance. All labels in m s^{-1}.

Fig. 4.7 shows, as contour lines, the simulated chloride ion concentration profile throughout a region close to the anode. The viscous layer becomes thicker towards the anode top, hindering chloride ion replenishment by convection and resulting in a thicker diffusion layer. The resultant lower chloride concentration at the anode surface produces increased concentration overpotential for this reaction (Eqn. 2.20). None of the previously published models take into account the variability of velocity and therefore velocity vectors along the cell gap height. This variation is critical due to the fact that it significantly affects the replenishment of chloride ions to the anode surface, which affects concentration overpotential and therefore the current density distribution.

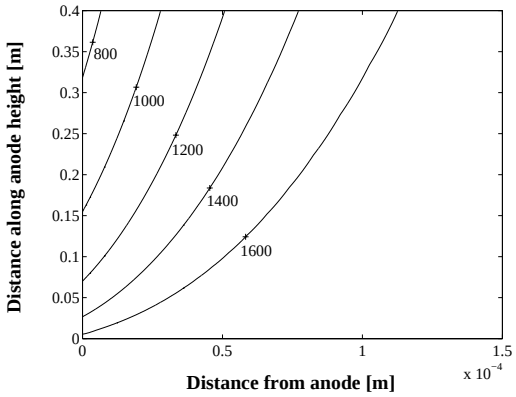

Fig. 4.7. The chloride ion concentration profile near the anode with a start velocity of 0.75 m s^{-1} and total current density of 2.5 kA m^{-2}. All labels in mol m^{-3}.

The current density distributions at three different velocities are shown in Fig. 4.8. Depleted ion concentration at the anode surface leads to less current at the top of the cell. At lower velocities, the current density distribution varies over a larger range than it does at greater velocities, due to the viscous layer being thicker.

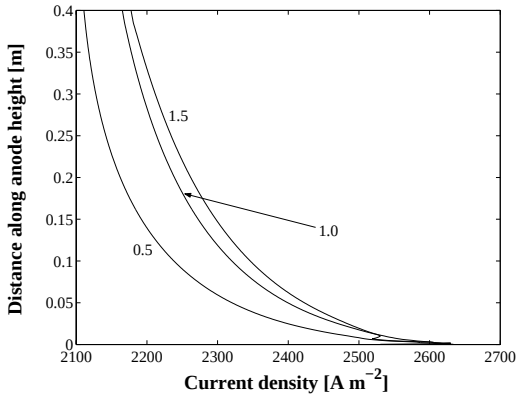

Fig. 4.8. The current density distribution at 0.5 m s^{-1}, 1.0 m s^{-1} and 1.5 m s^{-1} modelled for the chloride electrolysis reaction in a cell with a start current density of 2.5 kA m^{-2}.

The side-reactions

Shown in Paper III is the current density distribution lost to the water-splitting side-reaction (Eqn. 2.27). This shows this reaction as insignificant, in terms of loss in current efficiency, and that the electrochemical decay of the hypochlorite ion or the hypochlorous acid molecule that is the largest contributor to oxygen production at the anode. Figs. 4.9 and 4.10 show the respective current density distributions when the model is run using the different oxygen-producing side-reactions, (2.24) and (2.25), over a range of velocities.

The total amount of current density partaking in the electrochemical decay of the hypochlorite ion is not greatly affected by the flowrate. In converse to this, flowrate has quite an influence on the rate of electrochemical decay of the hypochlorous acid molecule (Fig. 9). Experience from the process indicates that oxygen production does not significantly vary through a large range of velocities, even when the process is run without the presence of sodium dichromate [7]. This leads to the conclusion that it is the side-reaction where the hypochlorite ion decays that is responsible for current efficiency loss in the chlorate process.

The local minimums in current density, seen in Fig. 4.9, are due to the developing viscous layer close to the anode and have not been mentioned previously in the literature. Initially, the inlet concentration of hypochlorite is uniformly distributed over the whole of the cell gap and reactants are readily available at the anode surface. Proceeding along the anode, the current density decreases as the hypochlorite ion surface concentration falls and hydrogen ion production increases. The effect of an increasing concentration overpotential, in the chlorine evolution reaction, then takes over and increases the rate of the side-reaction again, bringing about the local minimum.

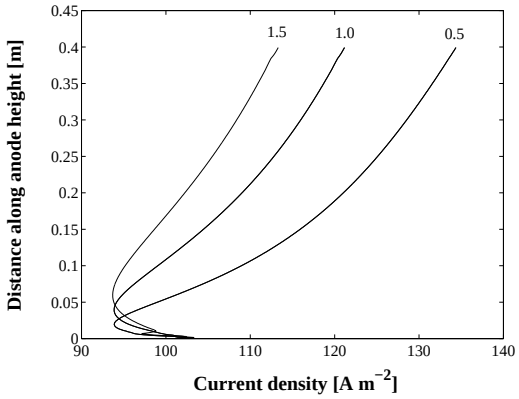

Fig. 4.9. The current density distribution for the electrochemical decay of the hypochlorite ion, Eqn. (2.24), at velocities of 0.5 m s^{-1}, 1.0 m s^{-1} and 1.5 m s^{-1}, modelled in a cell with a start current density of 2.5 kA m^{-2}. The exchange current density of the hypochlorite ion reaction is adjusted so as to guarantee a 2% - 4% oxygen production.

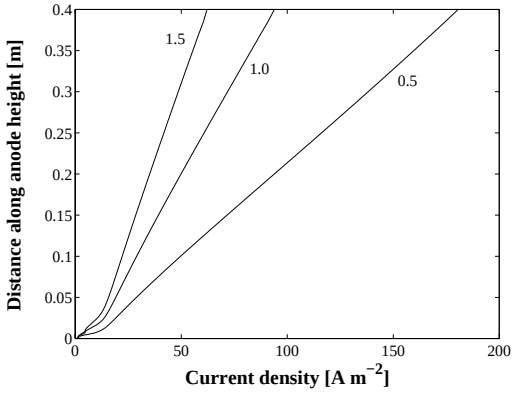

Fig. 4.10. The current density distribution for the electrochemical decay of the hypochlorous acid molecule, Eqn. (2.25), at velocities of 0.5 m s^{-1}, 1.0 m s^{-1} and 1.5 m s^{-1}, modelled in a cell with a start current density of 2.5 kA m^{-2}. The exchange current density of the hypochlorous acid molecule reaction is adjusted so as to guarantee a 2% - 4% oxygen production.

4.3. Simulations from a chlorate cell

Cell voltage and total current as a function of flowrate

The main investigation of the experimental cell was to study the effect of hydrodynamics on the electrolytic behaviour of the chlorate system. The thesis represents the cell hydrodynamics in terms of Reynolds number, in which cell gap flowrate and velocity can be calculated according to:

$$\mathrm{Re} = \frac{u_{\mathrm{av}} d_{\mathrm{h}} \rho}{\mu} \tag{4.1}$$

where u_{av} is the average velocity in the cell gap, ρ is the fluid density, μ is the fluid viscosity and d_{h} is the hydraulic diameter, given by:

$$d_{\mathrm{h}} = \frac{4 \cdot wl}{2 \cdot (w + l)} \tag{4.2}$$

where w is the cell gap width and l is the depth of the rectangular cell. The electrolyte viscosity was set to 1.22×10^{-3} N s m^{-2} and the density to 1.4×10^{3} kg m^{-3}, both typical values from industry [8].

An investigation of the hydrodynamic effects on both the anode and cathode was achieved by measuring the voltage between each respective electrode, and a reference electrode placed at a point in the cell gap centre. Fig. 4.11 shows the anodic (left) and cathodic voltages, from a galvanostatic trial, over a series of increasing Reynolds numbers. The results showed that by increasing flowrate, voltage decreased on the anodic side of the cell far more than it increased (decreased in the cathodic sense) on the cathodic side. This means that the anodic reaction was more enhanced by flowrate than the cathodic reaction.

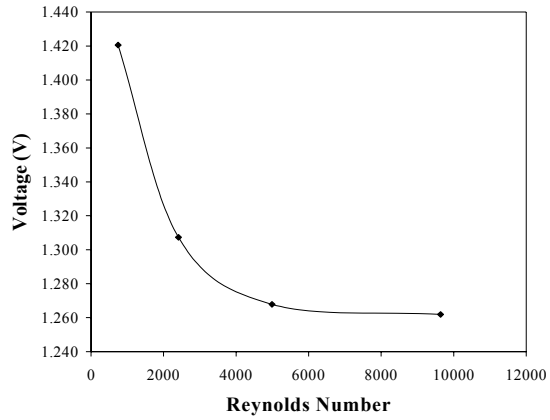

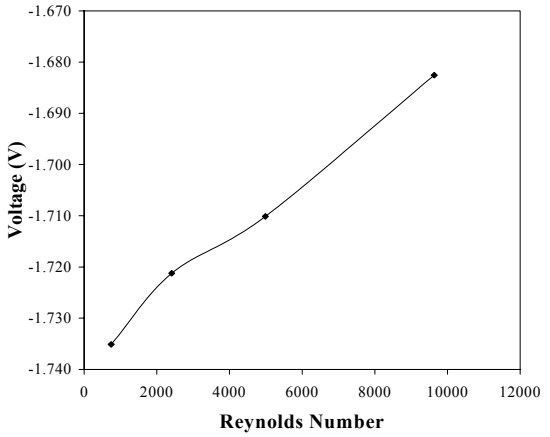

Fig 4.11. Potential drop between the anode (top) and the cathode (bottom) and reference electrode placed at a point in the center of the cell gap. The trial was run galvanostatically with the total current set at 2.32 kA m^{-2}. The electrolyte contained 503 g l^{-1} $NaClO_3$, 91.5 g l^{-1} NaCl and 1.9 g l^{-1} NaOCl, at a temperature of 63°C.

Increasing the flowrate along an electrode has the general effect of promoting mass transfer to the electrode surfaces, whilst also reducing the resistance caused by gas bubbles, as they are flushed through the cell at a quicker rate [37 – 39 & 43]. Yet, the results show that increasing flowrate enhanced the anodic side more than the cathodic side, which means that improvements to

the system as a whole depended more on concentration overpotential at the anode, than on how quick bubbles could be flushed from the cell.

Fig. 4.12 shows the cell voltage and its relation to flowrate in a galvanostatic trial. Three different regions in the diagrams are apparent. Initially, the cell voltage has a low value at very low Reynolds numbers, which reaches a maximum value as flowrate increases before it decreases again. The conclusion here is that the mixing and general turbulent effects of bubble evolution enhances the mass transfer of reacting species to electrode surfaces at these low Reynolds numbers. These effects decrease as flowrate increases and the electrolyte viscosity takes hold of the bubbles and flow becomes laminar in behaviour [42].

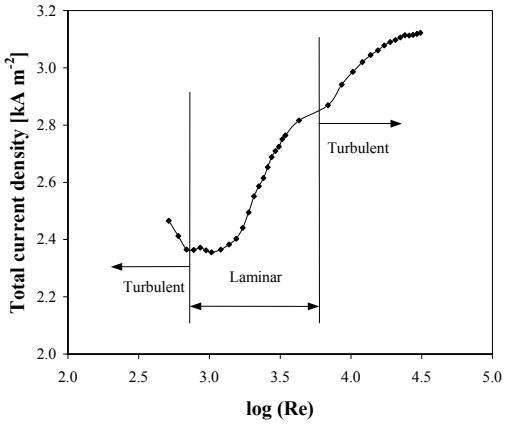

Fig. 4.12. The effect of the hydrodynamics (log of the Reynolds number) on total current from a potentiostatic trail. The electrolyte contained 503 g l^{-1} $NaClO_3$, 91.5 g l^{-1} NaCl and 1.9 g l^{-1} NaOCl, at a temperature of 63°C.

After the maximum, mass transfer is enhanced by a better replenishment of reacting species in the vicinity of the surface as flowrate increases. At moderate to high Reynolds numbers, the shape of the figure changes again, and the rate of decreasing cell voltage tapers off. It is in this region turbulent flow behaviour takes over, and an essentially uniform diffusion layer develops along the height of the electrode. This description of the hydrodynamic behaviour in the different regions is additionally discussion in relation to results with pressure drop measurements, presented in Paper IV.

Current density distribution as a function of flowrate

The effect of hydrodynamic behaviour on current density distribution was firstly studied through electrolysing a known solution of Iron(II) and Iron(III) hexacyanide ions ($Fe(CN)_6^{4-}$ and $Fe(CN)_6^{3-}$). The diffusion layer thickness could then be calculated from these results and is presented in Paper IV. What the results clearly show is that the diffusion layer thickness decreases geometrically along the height of the electrodes at low flowrates, and is basically uniform at high flowrates.

Fig. 4.13 shows a potentiostatic trial and Fig. 4.14 a galvanostatic trial where the current density distribution is presented at different Reynolds numbers. The figures show that the current density distribution is greater towards the bottom of the electrode length, which is particularly apparent at the lower flowrates when the hydrodynamic behaviour is laminar.

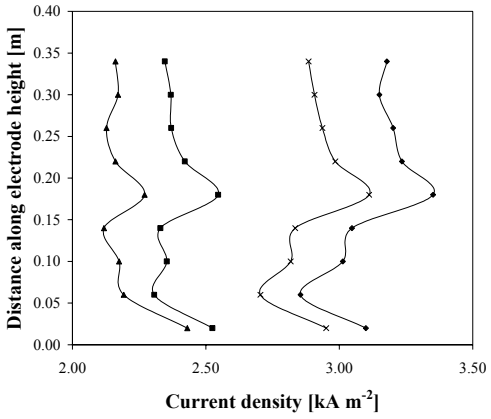

Fig. 4.13. Current density distribution at the anode from a potentiostatic trial electrolysing a chlorate electrolyte. The cell voltage was set at a value of 3.25 V, and the flow was varied according to the following Reynolds numbers: 774 (~ 0.1 m s^{-1} - ▲), 1893 (~ 0.25 m s^{-1} - ■), 3786 (~ 0.5 m s^{-1} - ×) and 8604 (~ 1.15 m s^{-1} - ◆). The electrolyte contained 556 g l^{-1} $NaClO_3$, 109 g l^{-1} NaCl and 1.2 g l^{-1} NaOCl, at a temperature of 60°C.

An assumed flat-line velocity profile enters the cell gap and contains an even distribution of reacting species. Before any viscous layer can develop along the electrode heights, large concentrations of the reacting species are present

in the vicinity of the surfaces, and the electrolytic reactions can easily take place. In the case of laminar flow, the hydrodynamic viscous layer develops along the cell gap height and hinders the transfer of reacting species to and from the electrode surfaces, producing a lower current.

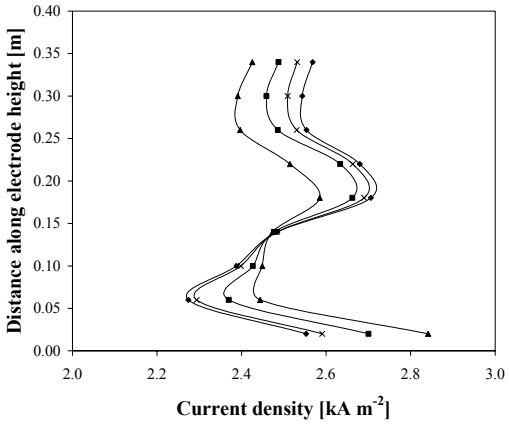

Fig. 4.14. Current density distribution at the anode from a galvanostatic trial electrolysing a chlorate electrolyte. The total current density was set at a value of 2.52 kA m^{-2}, and the flow was varied according to the following Reynolds numbers: 743 (~ 0.1 m s^{-1} - ▲), 1859 (~ 0.25 m s^{-1} - ■), 3700 (~ 0.5 m s^{-1} - ×) and 7400 (~ 1.0 m s^{-1} - ◆). The electrolyte contained 556 g l^{-1} $NaClO_3$, 109 g l^{-1} NaCl and 1.2 g l^{-1} NaOCl, at a temperature of 64°C.

Comparison of the results with the model

A comparison of results from the trials and mathematical model is presented in Fig. 4.15. This gives a better indication of the deficiencies in the experimental investigation than of the accuracy of the model. An encouraging result is that the model and results agree fairly well with each other at low flowrates and at the leading edge region of the electrode. Deviations from the model results at the higher part of the electrode show that a flow disturbance was occurring about midway along the electrode height. At greater flowrates, results from the cell and model do not agree very well with each other, which led us to the conclusion that the model cannot describe a system that could well be behaving in a turbulent fashion.

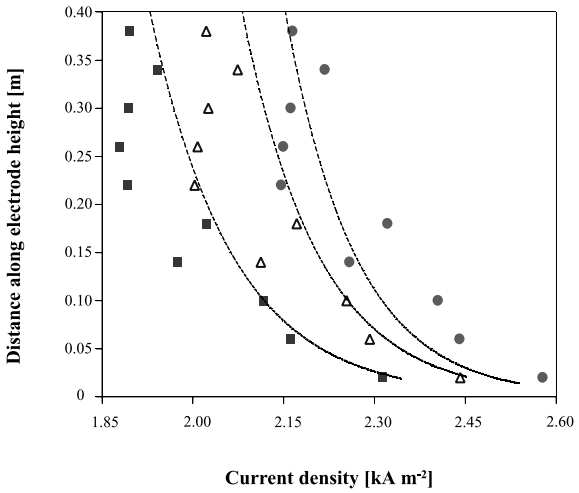

Fig. 4.15. Comparison of the model with results from a potentiostatic trial. The cell was run at Reynolds numbers of : 1858 (~ 0.25 m s^{-1} - ■), 5573 (~ 0.75 m s^{-1} - △) and 11145 (~ 1.5 m s^{-1} - ◆). Diagram taken from [59].

4.4. Simulations from a small electrochemical cell

Visualisation trials

Visualisation trials were useful in achieving a qualitative view of the system, and presented in Paper V are results that indicate that bubbles stayed confined to the electrode. It was postulated from these results that there existed three regions in the fluid beside a bubble-evolving electrode. These were:

- an adherence region, about the size of an average bubble diameter
- a bubbly region, which is very concentrated and in which bubbles diffuse to the bulk
- a bulk region, which contains clusters of bubbles that arrive there through jumping from the electrode surface after coalescence [43].

Velocity profiles

LDV measurements were impossible in the adherence region of the bubble layer because of the high bubble concentrations, and they first became accurate at between 200 μm and 300 μm from the electrode surfaces.

A velocity profile from the electrolysis of sodium sulphate is shown in Fig. 4.16 where the anode is on the left and the cathode on the right of the diagram. The different profiles were measured from different positions along the height of the cell, according to the description given in Fig. 3.2. What can be concluded from the diagram is that the curve went from a parabolic shape to a flatter curve with an 'M' profile. This means that the fluid adjacent to the bubble swarms moved faster than that in the centre of the cell.

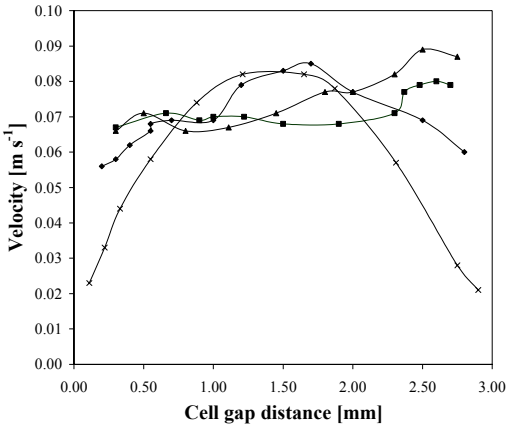

Fig. 4.16. Velocity profiles across the small electrochemical cell gap at a current density of 1000 A m^{-2}, in a Na_2SO_4 (50 g l^{-1}) electrolyte measured at: Position 1 (×), Position 2 (◆), Position 3 (■) and Position 4 (▲).

Velocity fluctuations and transition to turbulence

Turbulent intensity is a statistical quantification of velocity fluctuations and provides a description of the extent of turbulent behaviour. The *RMS* of the velocity fluctuations was measured at all four positions in the bubble layer,

for the three current densities: j = 500, 1000, and 2000 A m^{-2}, and in the centre of the cell gap at j = 1000 A m^{-2}. It was then normalised by the mean velocity in the cell gap to give us the turbulent intensity at these points, shown in Fig. 4.17.

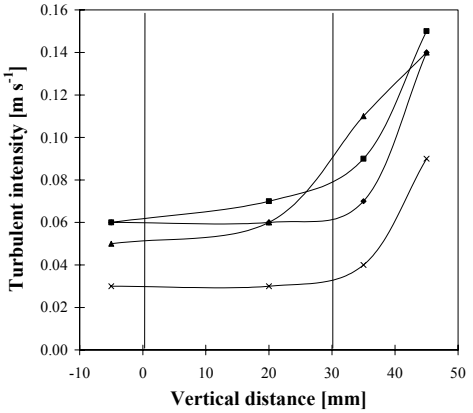

Fig. 4.17. Turbulent intensity evolution, in the bubble layer, along the cathode height for the three current densities of: j = 500 (⬥), 1000 (■), 2000 (●) A m^{-2} in an Na_2SO_4 (50 g l^{-1}) solution. The turbulent intensity in the centre of the cell gap, for j = 1000 (×) A m^{-2}, is also given, and the solid vertical lines indicate the placement of the entrance to and exit from the cell gap.

Boissonneau [58 & 60] measured turbulent intensity and found it to be around 10% in a turbulent boundary layer. Therefore, at positions 3 and 4 where turbulent intensity was in the range of 10% to 15 %, flow has a turbulent behaviour for the cases of the highest current densities of 1000 A m^{-2} and 2000 A m^{-2}. Transition between laminar and turbulent flows occurs at different locations along the cathode height, depending on the respective current densities. This transition was also noticeable from the PIV measurements, presented in Paper V. Turbulent intensity in the centre of the cell gap was far less than in the bubble layer. This also means that both turbulent and laminar behaviour can exist at the same horizontal plane.

5. CONCLUSIONS

The chlorate and chlor-alkali processes depend upon the mass transfer of species moving to and from electrode surfaces, and therefore the hydrodynamic behaviour of their systems. Improvements in this can increase the uniformity of current density distributions, at the respective electrodes, and reduce electrical energy, side-reaction incidence and electrocatalytic layer depletion. This thesis has presented results from studies involving mathematical modelling and experimental investigations of these processes.

It presented results from primary, secondary and psuedo-tertiary current density distribution models of a chlor-alkali anode the following was seen:

- electrolyte and membrane resistance have a far greater effect on current density distribution than electrode kinetics and mass transport
- mass transport has a certain effect on current density distribution, but a far greater effect on potential distribution
- in order to gain a more realistic model, the pseudo-tertiary current distribution model should be developed to include the migratory effects of the chloride ion in the diffusion layer, the ohmic effects of gas bubble adhesion and the variable size of the diffusion layer due to the macroconvection of electrolyte flow and the microconvection of gas evolution.

The thesis also presented results from a rigorous tertiary current density distribution model of the chlorate cell, which took into account the developing hydrodynamic behaviour along the height of the cell. This showed the following:

- concentration overpotential increases along the anode height, which leads to a decrease in the localized current density
- concentration overpotential becomes less extreme at greater velocities, so that current density distribution is more uniform
- a greater exchange current density reduces the overpotential term and allows a more uniform distribution of current density
- the fact that oxygen production does not vary greatly against flowrate points to the conclusion that it is the hypochlorite ion that partakes in the major side-reaction.

In order to experimentally investigate the chlorate cell, a real-scale cross-section of a segmented anode-cathode pair was investigated in industrial conditions. These experiments showed the following:

- an increase in flowrate equalized the uniformity of current density distribution
- concentration overpotential for the anode reaction, rather than the presence of hydrogen bubbles, steered the relationship between hydrodynamics and current density distribution
- flowrate increase brought about increases in mass transfer, reducing cell voltage and increasing total current
- three global hydrodynamic behaviours are apparent, depending on flowrate. At low velocities, turbulent behaviour was seen, followed by laminar behaviour and then turbulent behaviour again, as flowrate increased
- results from the cell and the model agree well with each other at lower flowrates and the leading part of the cell.

Finally, experiments involving bubble-induced free convection in a small electrochemical cell were investigated. These experiments showed the following:

- Laser Doppler Velocimetry is the most robust method for measuring such systems
- fluid flow in systems with bubble evolution can transform from laminar to turbulent behaviour throughout the height of a cell
- both turbulent and laminar behaviour can exist across the cell gap at the same horizontal plane

6. REFERENCES

1. A.D. Martin and A.A. Wragg, *"Numerical Modelling of Membrane Cell Primary Current and Potential Distributions. Part 2: Membrane Position, Electrode Position and Electrolyte Effects"*, 4th European Symposium on Electrochemical Engineering, Prague, Czech Republic, (1986).

2. K. Borucinski and K. Schneiders, *"A New Generation of the Krupp Udhe Single-Element Design"*, Modern Chlor-Alkali Technology, **Vol. 7**, Chap 13, Ellis Horwood (1996).

3. A.D. Martin, A.A. Wragg and J.C.R. Turner, *"Numerical Modelling of Membrane Cell Primary Current and Potential Distributions. Part 1: Finite Difference Approach and Effect of Electrode Shape",* IChemE Symposium Series No. **98**, (1986) 35.

4. J.T. Keating, *"Sulphate Deposition and Current Distribution in Membranes for Chlor-Alkali Cells"*, Proceedings from the Symposium on Electrochemical Engineering in the Chlor-Alkali and Chlorate Industries, Electrochemical Society, (1988).

5. J.S. Newman, *Electrochemical Systems*, 2nd edn., Prentice-Hall, Englewood Cliffs, NJ, (1991).

6. B.V. Tilak, in *Chlor-Alkali and Chlorate Technology*, H.S. Burney, N. Furuya, F. Hine and K.I. Ota, Editors, **PV 99-21**, p. 8, The Electrochemical Society Proceedings Series, Pennington, NJ (1999).

7. Discussions with N. Larsson, Permascand AB, Ljungaverk, Sweden.

8. Discussions with F. Herlitz, Eka Chemical AB, Sundsvall, Sweden.

9. N. Ibl and D. Landolt, *J. Electrochem. Soc*., **115**, 713 (1968).

10. D. Landolt and N. Ibl, *Electrochim. Acta*, **15**, 1165 (1970).

11. J. Venczel, *PhD Thesis*, Eidgenössische Technische Hochschule, Zürich, Switzerland, Prom no. **3673** (1965).

12. N. Ibl and J. Venczel, *Met. Oberfläche.*, **24**, 365 (1970).

13. T. R. Beck, *J. Electrochem. Soc*., **116**, 1038 (1969).

14. M.M. Jaksic, B.Z. Nikolic, I.M. Csonka and A.B. Djordjevic, *J. Electrochem. Soc*. **116**, 684 (1969).

15. M.M. Jaksic, A.R. Despic, I.M. Csonka and B.Z. Nikolic, *J. Electrochem. Soc*., **116**, 1316 (1969).

16. A.R. Despic, M.M. Jaksic and B.Z. Nikolic, *Jnl. Appl. Electrochem.*, **2**, 337 (1972).

17. M.M. Jaksic, *Jnl. Appl. Electrochem.*, **3**, 307 (1973).

18. M.M. Jaksic, *J. Electrochem. Soc*., **121**, 70 (1974).

19. M.M. Jaksic, *Electrochim. Acta*, **21**, 1127 (1976).

20. G.R. Heal, A.. Kuhn and R.B. Lartey, *J. Electrochem. Soc*., **124**, 1960 (1977).

21. B. Levich, *Physiochemical Hydrodynamics*, Prentice-Hall Inc, Eaglewood Cliffs, N. J. (1962).

22. L.J.J. Janssen and J.G Hoogland, *Electrochim. Acta,* **15**, 1013 (1970).

23. C. Boxall and G.H. Kelsall, *ICHEME Symposium series* nr **127**, 59 (1992).

24. H. Vogt, *Jnl. of Appl. Electrochem.*, **22**, 1185 (1992).

25. H. Vogt, *Electrochim. Acta*, **39**, 2173 (1994).

26. P. Ozil, M. Aurousseau and S. Mitu in *Transfer Phenomena in Magnetohydrodynamic and Electroconducting Flows,* A. Alemany, P. Marty and J.P. Thibault, Editors, p. 153, Kluwer Academic Publishers, The Netherlands (1999).

27. R. Wedin, *Licentiate Thesis*, Faxénlaboratoriet, Kungliga Tekniska Högskolan, Stockholm, Sweden (1999).

28. R. Leah, N.P. Brandon, V. Vesovic and G.H. Kelsall in *Abstracts from the 197th meeting of The Electrochemical Society*, Toronto, Canada, May 14 - 18 2000, Session **P1** (2000).

29. J.E. Funk and J.F. Thorpe, *J. Electrochem. Soc*. **116**, 48 (1969).

30. F. Hine and K. Murakami, *J. Electrochem. Soc*. **127**, 292 (1980).

31. B.E. Bongenaar-Schlenter, *PhD Thesis*, De Technische Universiteit, Eindhoven, The Netherlands (1984).

32. L.J.J. Janssen and G.J. Visser, *Jnl. of Appl. Electrochem.*, **21**, 753 (1991).

33. J.M. Bisang, *Jnl. of Appl. Electrochem.*, **21**, 760 (1991).

34. K. Scott, W. Taama and B.R. Williams, *Jnl. of Appl. Electrochem.*, **28**, 259 (1998).

35. R. Alkire and P. Lu, *J. Electrochem. Soc*. **126**, 2118 (1979).

36. H.F.M. Gijsbers and L.J.J. Janssen, *Jnl. of Appl. Electrochem.*, **19**, 637 (1989).

37. L.R. Czarnetzki, *PhD Thesis*, De Technische Universiteit, Eindhoven, The Netherlands (1989).

38. L.R. Czarnetzki and L.J.J. Janssen, *Jnl. of Appl. Electrochem.*, **19**, 630 (1989).

39. H. Vogt, in *Comprehensive Treatise of Electrochemistry*, B.E. Conway, J.O'M. Bockris, E. Yeager, S.U.M. Khan and R.E. White, Editors, **Vol. 6**, pps. 445- 489, Plenum Press, New York (1983).

40. H. Vogt, *Electrochim. Acta* **29** (1984) 167.

41. H. Vogt, *ibid*. **29** (1984) 175.

42. J.P. Prince and H.W. Blanch, *AI Chem. Eng. J.* **36** (1990) 1485.

43. L.J.J. Janssen, *Electrochim. Acta* **34** (1989) 161.

44. D. Ziegler and J.W. Evans, *J. Electrochem. Soc*. **133** (1986) 567.

45. A.J. Bard, in *Encyclopedia of Electrochemistry of the Elements*, **Vol. 1**, Marcel Dekker, New York, (1973).

46. S. Rondinini, M. Ferrari, "*Resistivity Behaviour of Perfluorinated Ionic Membranes in the Chlor-Alkali Electrolytic Process*", **PV 86-13**, Electrochemical Society, (1986).

47. D. Simonsson and G. Lindbergh, *Elektrokemi och korrosion*, Applied Electrochemistry, Royal Institute of Technology, Stockholm, (1997).

48. F. Foerster, *Trans. Am. Electrochem. Soc.*, **46**, 23 (1924).

49. K.L. Hardee and L.K. Mitchell, *J. Electrochem. Soc*., **136**, 3314 (1989).

50. S. Kotowski and B. Busse in *Modern Chlor-alkali Technology*. **Vol. 3**, Chap. 1, Ellis Horwood Ltd, Chichester (1986).

51. R.B. Bird, W.E. Stewart and E.N. Lightfoot, in *Transport Phenomena*, p. 71, John Wiley & Sons, New York, 1960.

52. B.V. Tilak, K. Tari and C.L. Hooper, *J. Electrochem. Soc*., **135**, 1386 (1988).

53. J. Aromaa, *PhD. Thesis*, Helsinki University of Technology, Espoo, Finland, **TKK-V-A12**, (1994).

54. M.S. Chao, *J. Electrochem. Soc*., **115**, 1172 (1968).

55. W.J. Moore, in *Basic Physical Chemistry*, p. 370, Prentice-Hall Inc., London (1986).

56. G. Peters, *Masters Thesis*, Institute for Applied Electrochemistry, Kungliga Tekniska Högskolan, Stockholm, Sweden (1993).

57. M.W. Lister, *Can. Jnl. of Chem.*, **34**, 479 (1956).

58. P. Boissonneau, *PhD. Thesis*, Université Joseph Fourier, Grenoble, France (1997).

59. Bosander P, Byrne P, Fontes E, & Parhammar O, “Current distribution on a membrane cell anode.” Published in *Chlor-Alkali and Chlorate Technology*, Burney, Furuya, Hine and Ota, Editors, **PV 99-21**, p. 45, The Electrochemical Society Proceedings Series, Pennington, NJ (1999).

60. P. Boissonneau and J.P. Thibault, in *Fluid Mechanics and its Applications. **Vol. 51**: Transfer Phenomena in Magnetohydrodynamic and Electroconducting Flows*, A. Alemany, Ph. Marty and J.P. Thibault, Editors, Kluwer Academic Publishers, Dordrecht, The Netherlands (1999).